# INVESTIGATIONS ON THE MECHANISM BEHIND THE BENEFICIAL EFFECT OF A FORMING GAS ANNEAL ON SOLAR CELLS WITH SILVER THICK FILM CONTACTS

G. Schubert[1], J. Horzel[2] and S. Ohl[1]
[1]University of Konstanz, Department of Physics, P.O.Box X916, D-78457 Konstanz, Germany
p: +49-7531-88-2088, f: +49-7531-88-3644, gunnar.schubert@uni-konstanz.de,
[2]SCHOTT Solar GmbH, Carl-Zeiss-Str. 4, 63755 Alzenau, Germany

ABSTRACT: In this contribution the beneficial effect of the forming gas anneal (FGA) on solar cells with silver thick film contacts is investigated regarding its application for contacting emitters with phosphorous surface concentrations below $N_{D,\,surface} = 1\times10^{20}$ cm$^{-3}$. Measurements and simulations of silver – silicon contacts show that for emitters with $N_{D,\,surface} > 2\times10^{19}$ cm$^{-3}$ the limiting factor for contacting is the current path from the silver crystals, grown onto the emitter, into the silver finger. The beneficial effect of the FGA on the fill factor (FF) of Si solar cells with screen-printed Ag contacts is found to be thermally activated at temperatures above 300°C and to be irreversibly stable in time. It is shown that the anneal affects the current path between silver crystals and finger. The formation of metal precipitates in the glass layer leading to an increase of the tunnelling probability and therefore lower contact resistance is suggested as the relevant mechanism behind the FF improvement. The results were successfully applied to fabricate solar cells with an emitter surface doping concentration of $N_{D,\,surface} < 5\times10^{19}$ cm$^{-3}$.
Keywords: silicon solar cell, thick film metallization, front contact

## 1 INTRODUCTION

Front side metallisation of n-type emitters of crystalline solar cells with silver thick film pastes is a well established technique in the photovoltaic industry. In the past years efforts were undertaken to get deeper insight in the formation and nature of silver thick film contacts (see e.g. [1-3]): The main goal is to develop lead free silver pastes with the ability to contact emitters with sheet resistances higher than 70 Ohm/sq and surface phosphorous concentrations below $1\times10^{20}$cm$^{-3}$. In this contribution the mechanism behind the beneficial effect of the forming gas anneal is investigated. Furthermore, it will be tried to apply the FGA for contacting solar cell emitters with phosphorous surface concentrations $N_{D,\,surface} << 1\times10^{20}$ cm$^{-3}$. The long term stability and the reversibility of the FGA improvement is studied.

## 2 REVIEW OF CONTACT FORMATION

Reviewing earlier investigations on the contact formation processes three main stages occur during contact formation (see Figure 1):

1. The glass contained in the Ag pastes is typically liquid at temperatures above 550°C. It etches through the $SiN_x$:H antireflection coating (ARC). Experiments on standard industrial solar cells (Cz, NaOH saw damage etch, 50 Ω/sq, full area Al back side, Ag front side) indicate that in a fast firing process a peak temperature of at least 750°C is necessary to penetrate the $SiN_x$:H layer completely.

2. Assuming a temperature high enough to enable the silver paste to penetrate the ARC homogenously, silver crystals are growing into the emitter, enhanced by a transfer process via reduced metals contained in the glass [4]. These crystals remain covered by a glass layer (see e.g. [5]) after temperature ramp-down of the contact firing step. The crystal growth depends mainly on the peak firing temperature and the surface phosphorous concentration of the emitter. On emitters with phosphorous concentrations below $N_D = 1\times10^{20}$cm$^{-3}$ peak firing temperatures higher than 800°C are necessary to achieve an adequate silver crystal coverage that is comparable to emitters with a high surface phosphorous concentration at $T_{peak} \approx 800$°C [1].

3. The average glass layer thickness, separating the silver crystals grown into the silicon from the bulk Ag contact finger, increases with increasing firing temperature [3, 6]. This effect leads to a greater distance between the silver crystals that are in direct contact with the emitter and the silver particles in the bulk of the contact finger. Additionally, sintering of the silver particles in the finger is enhanced with increasing firing temperature.

4. High firing temperatures lead to a reduction of the fill factor: metal impurities (e.g. silver from the tip of the crystals) diffuse towards the pn junction, increasing the recombination in the space charge region. Schottky-like shunting may occur and the ohmic shunt resistance may decrease due to excessive etching of the glass frit. Beside the peak firing temperature these effects depend on the doping profile [7].

## 3 LIMITING FACTORS FOR THE CURRENT TRANSPORT

Following the contact formation model described above the current transport from the emitter into the silver thick film contact is therefore mainly limited by two factors: 1. the contact resistivity of the silver crystals to the emitter and 2. the resistance for the current transport from these Ag crystals via the glass layer into the bulk of the silver fingers.

The contact resistivity of the silver crystals to an n-type emitter depends on the doping concentration. The current transport from these crystals into the bulk of the silver fingers occurs either via direct interconnections or via electron tunneling through the glass layers at locations where the layer is thin enough. Therefore, the number and size of the silver crystals and the average thickness of the glass layer determine the resistivity.

In case of emitters with a surface phosphorous

concentration below $1\times10^{20}$ cm$^{-3}$ the contact resistivity is therefore either limited by the number and size of the silver crystals grown into the emitter or by the reduced probability for efficient current paths through thick glass layers forming at elevated firing temperatures (see Figure 1).

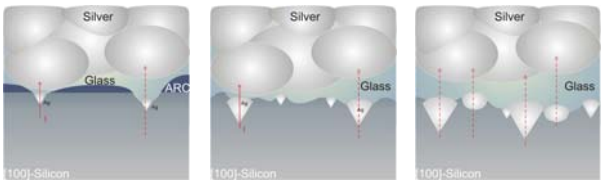


(a) $T_{peak} < 750°C$ (b) $T_{peak} \approx 800°C$ (c) $T_{peak} > 800°C$

**Figure 1:** Current transport model. (a) The glass has not penetrated the $SiN_x$ layer completely. (b) The ARC has been penetrated but only a few small crystals are grown at this peak temperature due to the reduced phosphorous surface concentration. (c) Higher firing temperatures lead to the growth of more and bigger crystals but the average glass layer thickness increases.

To identify the limiting factor in the current transport to moderately doped n-type silicon the electrical properties of these contacts were investigated.

Homogeneously phosphorous doped, polished, <100> oriented n-type silicon samples with a thickness of 380 µm and doping concentration of $N_D = 6\times10^{19}$ cm$^{-3}$ ($R_{sheet} = (0.034 \pm 0.009)$ Ω/sq) were selected. After printing the front grid (finger width after firing: 130 µm, finger spacing: 2.64 mm), using a commercially available Ag paste, the samples were fired in a rapid thermal processing furnace at $T_1 = 770°C$ and $T_2 = 850°C$. The dwell time was in both cases 30 s.

To separate the two possible limiting current paths two 1 cm wide stripes were cut out of these samples perpendicular to the fingers. The contact resistance was measured with the transmission line method (TLM) setup. After that, the silver fingers were removed in diluted HF (2% for 2 – 5 min). Only the silver crystals grown into the silicon remained, which was confirmed by SEM and EDX measurements. The number and size of the grown crystals were determined from SEM pictures. Then, liquid conductive silver was deposited on the silver crystals. A drying step was performed for 1 min at 50°C and the contact resistance was again measured using the TLM measurement setup. The electrical contact area was assumed to be the same as prior to etching the sintered finger although the conductive silver covered more than the original finger area. Therefore, the selectivity of this contacting method had to be tested by applying liquid conductive Ag on the bare surface of the substrates.

Finally, the influence of the forming gas anneal was tested by annealing the TLM samples in a tube furnace at 400°C (measured inside the tube) for 15 min in Ar-H(10%) atmosphere.

### 3.1 Crystal growth

Figure 2 shows representative SEM pictures of the silicon surface after removal of the silver fingers. In case of sample 1, fired at 770°C, only a few and very small silver crystals have grown into the silicon. However, the edge regions of the original fingers are covered by a large number of crystals. The surface of sample 2, fired at 850°C, is covered by many large crystals. As the conductive silver finger also contacts the edge crystals, the silver crystal coverage fraction, determined at six independent positions for each sample, has to be analysed carefully. The coverage for sample 2 is (23.5 ± 2.2)%, independently whether the Ag crystals from the original finger edges are included. In case of sample 1, the Ag crystal coverage in the middle of the finger is only (0.9 ± 0.3)%. Including the silver crystals at the finger edges, the coverage fraction was determined to be (2.7 ± 0.9)%. Assuming that only the edge crystals would contribute to the current transport and thus the electrical active finger width would be reduced to the width of the edge region covered by crystals, the coverage fraction of the edge crystals alone was determined to be (6.7 ± 0.9)%.

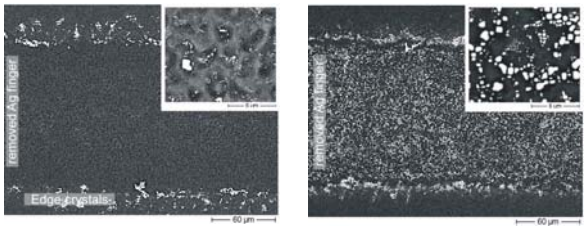


(a) $T_{peak} = 770°C$ (b) $T_{peak} = 850°C$

**Figure 2:** SEM top view pictures of two samples after removal of the silver finger. The silver crystals grown into the silicon are clearly visible (white spots).

### 3.2 Electrical properties

After firing, the measured contact resistance values were much higher than the possible emitter contribution to the total resistance. Independent of the finger distance average resistance values of (123 ± 24) Ω and (48 ± 17) Ω were measured for samples 1 and 2, respectively. As the maximal emitter contribution ($R_{emitter,\ max} = 0.036$ Ω) can be neglected, the measured resistance can be approximated to be twice the contact resistance $R_C$. After removal of the silver grid and depositing liquid conductive silver on the remaining silver crystals, the measured resistance values dropped drastically. In both cases the contact resistance was in the order of magnitude of the sheet resistance so that the transfer length model was applied to extract the contact resistivity. $\rho_{C,1} = (0.094 \pm 0.002)$ mΩcm$^{-2}$ and $\rho_{C,2} = (0.047 \pm 0.018)$ mΩcm$^{-2}$ were extracted for samples 1 and 2, respectively. These resistivity values differ by a factor of 2. In both cases these resistivity values are low enough to be excluded as FF limiting factor. That the contact resistivity value of sample 1 is only twice that of sample 2 despite the significantly lower Ag crystal density on sample 1 is confirming this conclusion.

As the conductive silver contacts the bare silicon areas between the crystals, the selectivity of this method was verified by directly applying the silver on the substrate at locations without any crystals. The total resistance was measured to be (51 ± 23) Ω independent of the distance between the areas that had been covered by liquid Ag. This is three orders of magnitude higher than the total resistance measured when contacting areas with the silver crystals present and therefore confirms the selectivity of this method.

3.3 Comparison with contact resistivity model

In Figure 3 the dependency of the contact resistivity on the doping concentration is plotted following the approach of Yu [8]. In the doping regime between $1\times10^{19}$ cm$^{-3}$ and $1\times10^{20}$ cm$^{-3}$ thermionic field emission is dominating. The simulations were performed with the tunnelling effective mass as the free parameter. As upper limit, $m_{tunnel}/m_e = 1$, was used taken from Schroder and Meier [9] whereas $m_{tunnel}/m_e = 0.3$, a more recent literature value given by Ng and Liu [10], was used as lower limit. The best fit for the results of the previous experiment is $m_{tunnel}/m_e = 0.51$ to 0.58. The resistivity for an average single Ag crystal was calculated by multiplying the measured value by the silver crystal covered surface area and a surface enlargement factor resulting from the pyramidal shape of the crystals.

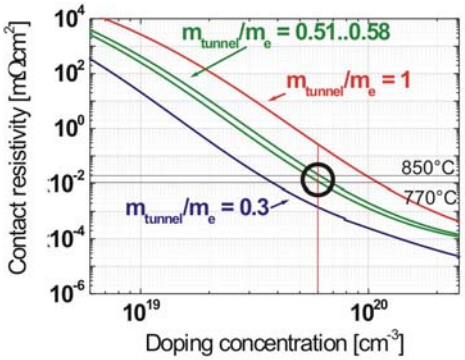


**Figure 3:** Contact resistivity in dependence of doping concentration. The experimentally determined values fit best with $m_{tunnel}/m_e$ = 0.51..0.58. Other parameters: barrier height $\phi_B = 0.78$ eV [11], effective Richardson constant $A^* = 112$ Am$^{-2}$K$^{-2}$ [12], T = 300 K, image force lowering

This simulation can be used to estimate the lower limit for an emitter surface phosphorous doping that can be contacted with silver. Assuming a 100% coverage and direct silver – finger interconnections a phosphorous surface concentration of $N_{D,surface} > 2\times10^{19}$ cm$^{-3}$ would result in $\rho_C < 1$ mΩcm$^2$, which would be low enough to guarantee fill factors above 77% on industrial solar cells.

3.4 Influence of the forming gas anneal

To get more insight in the mechanism behind the beneficial effect of the forming gas anneal [14] the contact resistance of a neighbouring TLM stripe of sample 2 was measured before and after the forming gas anneal. As the contribution of the sample to the total resistance is again negligible, the measured resistance can again be approximated to be $2xR_C$. In Figure 4 the results are presented. The forming gas anneal leads to a decrease in $R_C$ to 1.7% of the resistance measured before annealing.

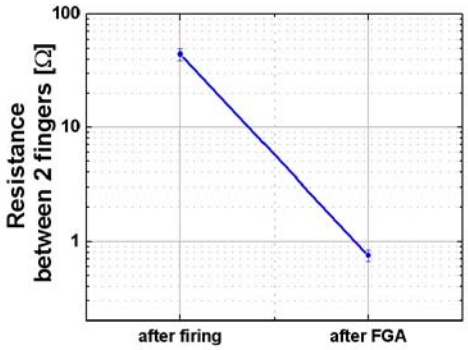


**Figure 4:** Resistance between two fingers before and after a forming gas anneal at 400°C for 15 min in Ar-H.

3.5 Discussion

From these results two important conclusions can be drawn:

1. The contact resisitivity of the silver crystals to an emitter with a surface doping concentration higher than $2\times10^{19}$ cm$^{-3}$ is not the limiting factor for the total contact resistance. The current path from the Ag crystals through the glass layer to the bulk of the Ag finger is the reason for high contact resistance values.

2. The forming gas anneal leads to a drastic decrease in the contact resistance. As the resulting resistance is still much higher than the contact resistance of the silver crystals to the silicon, it can be deduced that the beneficial effect of the FGA affects the current path from the Ag crystals into the bulk of the Ag finger.

## 4 MACROSCOPIC EFFECTS

To get a deeper insight in the mechanisms of the forming gas anneal, the macroscopic effects of the forming gas anneal were studied. The investigations were performed using standard industrial 12.5×12.5 cm$^2$ solar cells on p-type Cz-Si with a NaOH saw damage etch, no additional texturisation of the surface, a $POCl_3$ diffusion to obtain sheet resistances of $R_{sheet} = (51.2 \pm 0.6)$ Ω/sq, and a $SiN_x$ antireflection coating. The front and rear side contacts have been screen-printed applying on the front side both, a standard commercially available, lead containing silver thick film paste and a lead free silver paste [13]. For the rear side a standard commercially available aluminium thick film paste has been applied. After drying, the pastes were fired in a conveyor belt furnace with three heating zones. The temperature of the third zone was varied. To account for light induced degradation of the Cz solar cells, these cells were annealed at 200°C for 20 min prior to the J-V measurements before and after FGA.

4.1 Cell results

In Figure 5 the solar cell parameters of under-fired ($T_{peak}$ = 745°C), optimal fired ($T_{peak}$ = 795°C) and extremely over-fired ($T_{peak}$ = 885°C) solar cells are shown before and after applying a standard forming gas anneal (Ar-H(10%), 400°C (inside tube), 15 min). Two cells per group were analysed. It is obvious that the fill factor is limiting the efficiency of not optimal fired solar cells prior to the forming gas anneal. After the forming gas anneal the fill factor of the over-fired solar cells is

more than doubled. The fill factors of the under-fired and optimal fired cells remain constant within the accuracy of measurement. The over-fired cells show an increase in $J_{sc}$. The increase in $J_{sc}$ of the under-fired cells is minor. The optimal fired cells do not show significant changes. Most of the cells show a little loss in Voc (0.1 to 0.3% relative) after the forming gas anneal (not plotted for clarity reasons). In total the efficiency is drastically increased in case of the extremely over-fired cells. The efficiency of the optimal fired cells is constant within the accuracy of measurement and the efficiency of the under-fired cells is increased due to the increase in $J_{sc}$.

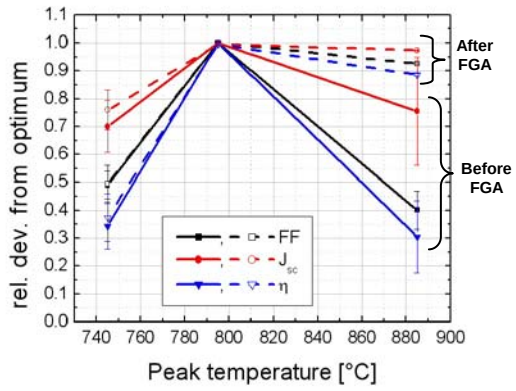


**Figure 5:** Relative deviation of FF, $J_{sc}$ and efficiency from optimum in dependence of the peak firing temperature prior to (full line) and after (dashed line) forming gas anneal at 400°C for 15 min.

Analysing the J-V characteristics revealed that the fill factor increase is attributed to the decrease in series resistance which in turn can be traced back to a decrease in the contact resistivity in accordance with previous studies [14]. No remarkable effect on the shunt resistance, diode saturation currents and effective diffusion length were detected for these samples. However, it cannot be excluded that a forming gas anneal can have effects on these parameters in solar cells with different emitter profiles, silver pastes or surface texturing. Furthermore, a beneficial effect of edge passivation due to Ar-H annealing was not observed but can not be excluded to occur.

4.2 Influence of atmosphere during anneal

Substituting the reducing Ar-H atmosphere with oxygen leads to a decrease in fill factor due to an increase in the contact resistivity. $N_2$ as the annealing gas was also found to have a negative effect on the contact resisitivity in accordance with Rohatgi et al. [15].

4.3 Long term stability

The long term stability of the beneficial effect of the forming gas anneal was tested on one cell for 17 months in comparison with a reference cell. In Figure 6 the evolution of the fill factor and the efficiency of the two industrial solar cells are plotted. Both cells were identically processed except for the used silver paste and firing conditions. In case of the over-fired cell a lead free silver paste was used. The reference cell was processed with a standard silver paste at optimal firing conditions. The forming gas anneal increased the fill factor of the overfired solar cell remarkably. After 17 months both solar cells are stable within the accuracy of measurement. The cells were stored in a box at room temperature in darkness.

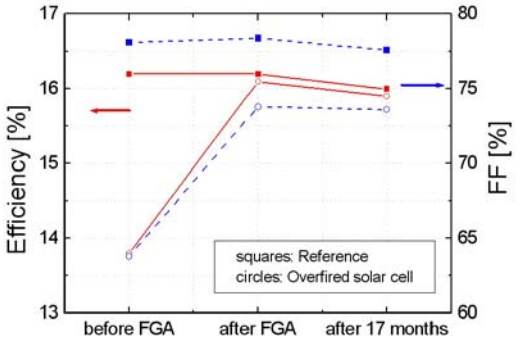


**Figure 6:** Long term stability of the beneficial effect of the forming gas anneal (FGA: Ar-H(10%), 400°C, 15 min)

It is interesting to note that the beneficial effect of the forming gas anneal seems to be irreversible. Applying an additional oxygen anneal at 400°C for 15 min after the forming gas anneal (400°C, 15 min) did not reverse the FGA improvement (Figure 7).

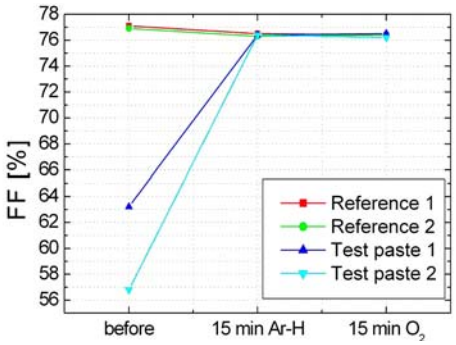


**Figure 7:** The beneficial effect of the forming gas anneal at 400°C was not reversible by annealing in $O_2$ atmosphere at 400°C.

4.4 Influence of annealing temperature and time

To get more insight in the processes occurring during the forming gas anneal, temperature and dwell time of the anneal were varied. In Figure 8 the development of the fill factor of a solar cell, fired at 845°C, is plotted versus subsequent annealing steps (15 min). The fill factor increases strongly at T = 375°C. A subsequent annealing step at 400°C did not lead to further improvements. Analysis of the diode parameters revealed that the fill factor is limited by $J_{02}$ ($J_{02}$ = 66 nA/cm$^2$). Applying forming gas annealing steps at 450°C or higher did not lead to improvements in the fill factor.

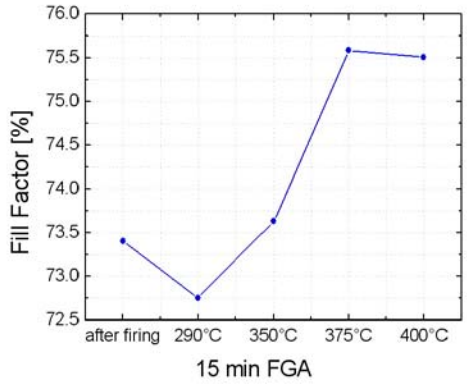


**Figure 8:** Subsequent forming gas annealing steps at different temperatures. The beneficial effect on the fill factor arises at T = 375°C.

Varying the dwell time during the forming gas anneal at 400°C showed that the process is time dependent. After 5 min the improvement from the FGA becomes noticeable. After 15 min the maximal improvement in the fill factor is reached. Annealing for longer times does not lead to further decrease in contact resistance.

4.5 Conclusion

Summarising these results, it is likely that a chemical reaction occurs during the forming gas anneal. A temperature of T = 375°C or higher is necessary to start the reaction on the investigated cells. Additionally, it was found that the reaction is not fast, compared to the contact formation processes in a rapid thermal firing sequence. It has to be pointed out that the forming gas anneal was applied to pastes with different glass frits characterised by different glass transformation temperatures. In all cases the forming gas anneal works best at T = 400°C. A reduction of the metal oxides in the glass by hydrogen from the FGA forming metallic precipitates is the most likely reaction occurring during the annealing step.

The formation of metallic precipitates in lead borosilicate glass during the forming gas anneal was observed in other studies. It was also observed that the distributed metal particles after the forming gas anneal lead to an increase in the surface conductivity of glass, especially if the glasses contain, beside lead oxide, bismuth oxide [16–18]. According to these publications, bismuth is supposed to act as a resonant centre for the resonant tunnelling conduction mechanism. In case of a limitation of $\rho_C$ by an increased glass layer thickness due to over-firing, it is therefore likely that the current transport between the silver crystals, grown into the emitter and the bulk of the Ag silver finger occurs via a multi-step tunnelling mechanism from precipitate to precipitate. The tunnelling probability through a thick glass layer is assumed to be increased by a forming gas anneal (Figure 9).

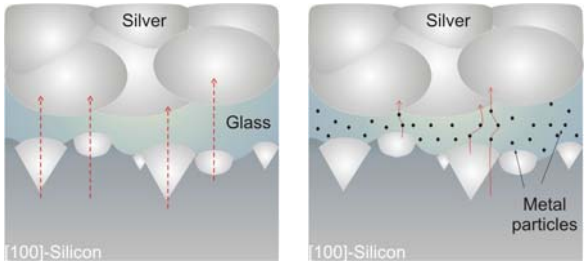


(a) over-fired contact (b) after FGA

**Figure 9:** (a) Over-fired silver thick film contact. The current transport is limited by the glass layer thickness. (b) The beneficial effect of the forming gas anneal originates most likely from a reduction of metal oxides in the glass layer and consequently an increased tunnelling probability due to a multi-step tunnelling mechanism.

## 5 APPLICATION TO SOLAR CELLS

As it was found that the forming gas anneal increases the conductivity of the separating layer between silver crystals, the FGA was applied to 5×5 $cm^2$ Cz industrial solar cells using three emitters differing in the phosphorous surface concentration. Drive-in steps were used in order to obtain deep profiles for the emitter P concentration. For processing details see also reference [1]. After emitter formation a $SiN_x$ layer was applied. The front contacts were screen-printed using a commercially available, leaded Ag paste, optimised for 40 - 60 Ω/sq emitters with high P surface concentrations. After printing the Al back contact, the samples were fired in an RTP furnace to ensure an accurate control of the process parameters. Three different peak firing temperature were used ($T_{peak1}$ = 810°C, $T_{peak2}$ = 835°C and $T_{peak3}$ = 860°C). Three samples per firing parameter and emitter were processed. Finally, a standard forming gas anneal (Ar-H(10%), 400°C, 15 min) was applied.

5.1 Emitter profiles

In Figure 10 the carrier concentration profiles of the three emitters measured with ECV are shown. The P surface concentrations of emitter 1, 2 and 3 are $1\times10^{20}$ $cm^{-3}$, $4\times10^{19}$ $cm^{-3}$ and $3\times10^{19}$ $cm^{-3}$, respectively.

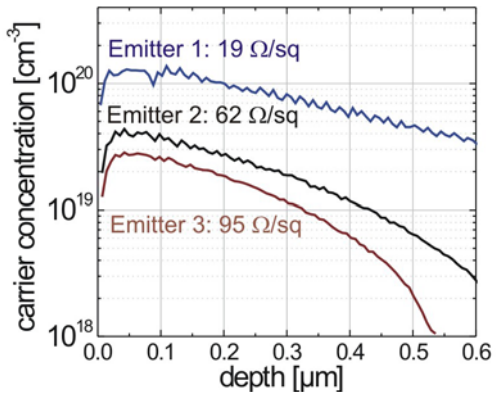


**Figure 10:** Electrical active phosphorous concentration for the three emitters measured with ECV.

5.2 Crystal coverage

One cell per parameter was used to determine the crystal coverage fractions from SEM pictures after removal of the silver grids in diluted HF. Figure 11

shows the determined coverage fractions in dependence of the firing temperature.

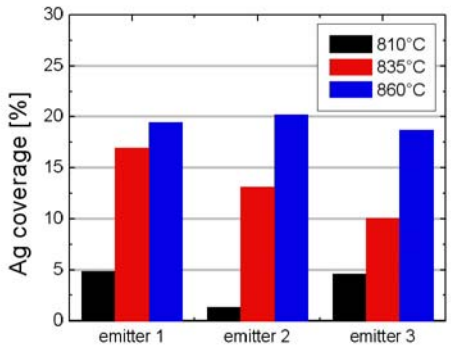


**Figure 11:** Crystal coverage fraction for different peak temperatures and emitter profiles.

At $T_{peak} = 810°C$, (optimal firing temperature for phosphorous surface concentrations exceeding $1\times10^{20}$ cm$^{-3}$), the crystal coverage fraction for Ag fingers on emitters with $N_{D,\,surface} < 1\times10^{20}$ cm$^{-3}$ is small. The Ag coverage increases with increasing firing temperatures. But as stated above the glass layer thickness increases as well.

5.3 Cell results

IV measurements after firing show that very low fill factors are achieved on all samples independent of the firing temperature (Figure 12).

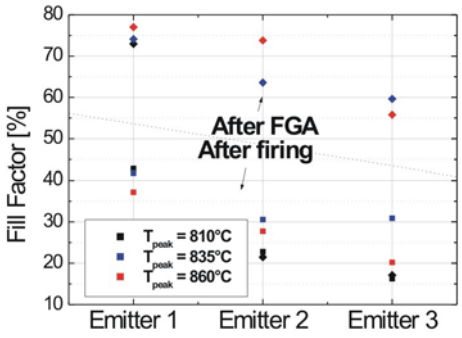


**Figure 12:** Fill factor before (squares) and after forming gas anneal (rhombuses).

After annealing in forming gas the cells with emitter profile 1 (high electrical active surface concentration) show a drastic improvement of the fill factors to values between 73% ($T_{peak} = 810°C$) and 77% ($T_{peak} = 860°C$) in contrast to 42% and 37% after firing. This result clearly indicates the dependency of the contact resistivity on the crystal coverage fraction. The solar cells with drive-in emitter 2 and 3 fired at $T_{peak} = 810°C$ do not show an increased fill factor. At $T_{peak} = 835°C$ the fill factor of cells with these emitter profiles doubles after the FGA. At $T_{peak} = 860°C$ the fill factor of cells with emitter profile 3 is not further increased. Further analysis showed a still high series resistance of $R_s \approx 4.5\ \Omega cm^2$ for this cell. The main loss factor is, however, the high second diode saturation current ($J_{02} = 180$ nA/cm$^2$). The origin is presumably metal impuritiy diffusion to the space charge region of the pn junction.

The best cell results were reached on the cell with emitter profile 2 with a higher junction depth and a slightly increased surface doping at $T_{peak} = 860°C$. The cell results are summarised in Table 1.

| | **FF [%]** | $J_{sc}$ [mA/cm$^2$] | $V_{oc}$ [mV] | η [%] |
|---|---|---|---|---|
| Best cell | **73.8** | 32.4 | 616.5 | 14.9 |

**Table 1:** Result of the solar cell with emitter 2 fired at 860°C after forming gas anneal.

Further analysis showed that the series resistance is not the limiting factor for the fill factor ($R_s = 0.68\ \Omega cm^2$). Again, the high second diode saturation current ($J_{02} = 84$ nA/cm$^2$) limits the fill factor and the open circuit voltage. With a reduced $J_{02}$ ($J_{02} = 20$ nA/cm$^2$) a fill factor of 77% could be expected.

The experiment proved that it is possible to fabricate solar cells with moderately phosphorous surface concentrations using silver thick film metallisation. Emitters with a surface phosphorous concentration of $N_{D,\,surface} = 4\times10^{19}$ cm$^{-3}$ were successfully contacted with a standard, commercially available silver paste. Further optimisation of both, the silver paste and the emitter profile, is necessary to avoid losses due to high second diode saturation currents.

## 6 SUMMARY

In this contribution it was shown that the current transport from the silver crystals to the silver finger is the limiting factor in silver thick film contacts to emitters with $2\times10^{19}$ cm$^{-3}$ < $N_{D,\,surface}$ < $1\times10^{20}$ cm$^{-3}$. This current path is determined by the number and size of the grown silver crystals and the average glass layer thickness.

The beneficial effect of the forming gas anneal was identified to be located in this transition region. As this effect is thermally activated and is only observed in a reducing atmosphere (Ar-H), it is reasonable to assume a reducing reaction of the metal oxides present in the glass layer with hydrogen of the forming gas. The decrease in contact resistance can then be traced back to an increased tunneling probability due to a multi-step tunneling mechanism from metal precipitate to precipitate. It was shown that the investigated industrial Cz solar cells improve in FF after FGA due to a lower contact resistance. Other parameters like the shunt resistance or the effective diffusion length were not influenced. These results were successfully applied to fabricate solar cells with a surface doping concentration of the emitter of $N_{D,\,surface} < 5\times19^{19}$cm$^{-3}$. A standard, commercially available silver paste was used. The best cell reached a fill factor of 73.8%, which was limited by the high second diode saturation current. Further optimisation of the emitter profile and the silver paste is expected to be a promising way to apply silver thick film metallisation to "high-efficiency" emitters with $N_{D,\,surface} < 1\times10^{20}$ cm$^{-3}$.


## ACKNOWLEDGEMENTS

We would like to thank R. Kopecek for the ECV measurements and C. Strümpel for fruitful discussions. The underlying project of parts of this paper was supported by funding by the EC under project No. ENK6-CT-2001-00560 (EC2Contact). The content of this publication is the responsibility of the authors.

REFERENCES


[1] G. Schubert, J. Horzel, R. Kopecek, F. Huster, and P. Fath, in Proc. 20th EC PVSEC, Barcelona, Spain, 2005, pp. 934–937.

[2] G. Grupp, D. M. Huljic, R. Preu, G. Willeke, and J. Luther, in Proc. 20th EC PVSEC, Barcelona, Spain, 2005, pp. 1379–1382.

[3] M. Hilali, M. Al-Jassim, B. To, H. Mountinho, A. Rohatgi, and S. Asher, Journal of the Electrochemical Society, vol. 152, no. 10, pp. G742–G749, 2005.

[4] G. Schubert, F. Huster, and P. Fath, in Proc. 19th EC PVSEC, Paris, France, 2004, pp. 813–816.

[5] C. Ballif, D. M. Huljic, G. Willeke, and A. Hessler-Wyser, Applied Physics Letters, vol. 82, no. 12, pp. 1878–1880, 2003.

[6] C. Khadilkar, S. Sridharan, D. Gnizak, T. Pham, S. Kim, and A. Shaikh, in Proc. 20th EC PVSEC, Barcelona, Spain, 2005, pp. 1291–1296.

[7] A. Bentzen, G. Schubert, J. S. Christensen, B. Svensson, and A. Holt, accepted for publication in Progress in Photovoltaics, 2006.

[8] A. Y. C. Yu, Solid State Electronics, vol. 13, pp. 239–247, 1970.

[9] D. K. Schroder and D. L. Meier, IEEE Transactions on Electron Devices, vol. 31, no. 5, pp. 637–647, 1984.

[10] K. K. Ng and R. Liu, IEEE Transaction on Electron Devices, vol. 37, no. 6, pp. 1535–1537, 1990.

[11] S. M. Sze, Physics of Semiconductor Devices. Inc. New York: John Wiley & Sons, 1981.

[12] J. M. Andrews and M. P. Lepselter, Solid-State Electronics, vol. 13, pp. 1011–1023, 1970.

[13] J. Hoornstra, G. Schubert, C. LePrince, G. Wahl, K. Broek, F. J. Granek, B. Lenkeit, and J. Horzel, in Proc. 20th EC PVSEC, Barcelona, 2005, pp. 651–654.

[14] T. Nakajima, A. Kawakami, and A. Tada, International Journal of Hybrid Microelectronics, vol. 6, no. 1, pp. 580–586, 1983.

[15] A. Rohatgi, S. Narasimha, and A. Ebong, Transactions on Electron Devices, vol. 46, no. 10, pp. 1970–1077, 1999.

[16] O. Gzowski, L. Murawski, and K. Trzebiatowski, Journal of Non-Crystalline Solids, vol. 41, pp. 267–271, 1980.

[17] M. Chybicki, J. Liwo, and K. Trzebiatowski, Physica Status Solidi A, vol. 115, pp. K185–K189, 1989.

[18] O. Gzowski, L. Murawski, and K. Trzebiatowski, Journal of Applied Physics, vol. 15, pp. 1097–1101, 1982